Biomedical Optics EXPRESS

Micro-ultrasonic cleaving of cell clusters by laser-generated focused ultrasound and its mechanisms

Hyoung Won Baac,[1,3] Taehwa Lee,[2] and L. Jay Guo[1,2,*]

[1]*Department of Electrical Engineering and Computer Science, University of Michigan, Ann Arbor, MI 48109, USA*
[2]*Department of Mechanical Engineering, University of Michigan, Ann Arbor, MI 48109, USA*
[3]*Currently with Harvard Medical School and Massachusetts General Hospital, Wellman Center for Photomedicine, Boston, MA 02114, USA*
[*]*guo@umich.edu*

Abstract: Laser-generated focused ultrasound (LGFU) is a unique modality that can produce single-pulsed cavitation and strong local disturbances on a tight focal spot (<100 μm). We utilize LGFU as a non-contact, non-thermal, high-precision tool to fractionate and cleave cell clusters cultured on glass substrates. Fractionation processes are investigated in detail, which confirms distinct cell behaviors in the focal center and the periphery of LGFU spot. For better understanding of local disturbances under LGFU, we use a high-speed laser-flash shadowgraphy technique and then fully visualize instantaneous microscopic processes from the ultrasound wave focusing to the micro-bubble collapse. Based on these visual evidences, we discuss possible mechanisms responsible for the focal and peripheral disruptions, such as a liquid jet-induced wall shear stress and shock emissions due to bubble collapse. The ultrasonic micro-fractionation is readily available for *in vitro* cell patterning and harvesting. Moreover, it is significant as a preliminary step towards high-precision surgery applications in future.

OCIS codes: (170.7170) Ultrasound; (170.0170) Medical optics and biotechnology.

References and links

1. G. T. Haar and C. Coussios, "High intensity focused ultrasound: physical principles and devices," Int. J. Hyperthermia **23**(2), 89–104 (2007).
2. C. C. Coussios and R. A. Roy, "Applications of acoustics and cavitation to noninvasive therapy and drug delivery," Annu. Rev. Fluid Mech. **40**(1), 395–420 (2008).
3. J. E. Lingeman, J. A. McAteer, E. Gnessin, and A. P. Evan, "Shock wave lithotripsy: advances in technology and technique," Nat Rev Urol **6**(12), 660–670 (2009).
4. J. J. Rassweiler, T. Knoll, K.-U. Köhrmann, J. A. McAteer, J. E. Lingeman, R. O. Cleveland, M. R. Bailey, and C. Chaussy, "Shock wave technology and application: an update," Eur. Urol. **59**(5), 784–796 (2011).
5. J. E. Kennedy, "High-intensity focused ultrasound in the treatment of solid tumours," Nat. Rev. Cancer **5**(4), 321–327 (2005).
6. Y.-F. Zhou, "High intensity focused ultrasound in clinical tumor ablation," World J Clin Oncol **2**(1), 8–27 (2011).
7. T. J. Dubinsky, C. Cuevas, M. K. Dighe, O. Kolokythas, and J. H. Hwang, "High-intensity focused ultrasound: current potential and oncologic applications," AJR Am. J. Roentgenol. **190**(1), 191–199 (2008).
8. C. Goldenstedt, A. Birer, D. Cathignol, and C. Lafon, "Blood clot disruption in vitro using shockwaves delivered by an extracorporeal generator after pre-exposure to lytic agent," Ultrasound Med. Biol. **35**(6), 985–990 (2009).
9. A. D. Maxwell, "Noninvasive thrombolysis using histotripsy pulsed ultrasound cavitation therapy," Ph.D. Thesis, University of Michigan (2012).
10. Z. Xu, A. Ludomirsky, L. Y. Eun, T. L. Hall, B. C. Tran, J. B. Fowlkes, and C. A. Cain, "Controlled ultrasound tissue erosion," IEEE Trans. Ultrason. Ferroelectr. Freq. Control **51**(6), 726–736 (2004).
11. Z. Xu, J. B. Fowlkes, E. D. Rothman, A. M. Levin, and C. A. Cain, "Controlled ultrasound tissue erosion: The role of dynamic interaction between insonation and microbubble activity," J. Acoust. Soc. Am. **117**(1), 424–435 (2005).
12. A. Maxwell, O. Sapozhnikov, M. Bailey, L. Crum, Z. Xu, B. Fowlkes, C. Cain, and V. Khokhlova, "Disintegration of tissue using high intensity focused ultrasound: two approaches that utilize shock waves," Acou. Today **8**(4), 24–37 (2012).

#187689 - $15.00 USD Received 25 Mar 2013; revised 3 Jul 2013; accepted 10 Jul 2013; published 26 Jul 2013

13. C.-D. Ohl and B. Wolfrum, "Detachment and sonoporation of adherent HeLa-cells by shock wave-induced cavitation," Biochim. Biophys. Acta **1624**(1-3), 131–138 (2003).
14. L. Junge, C. D. Ohl, B. Wolfrum, M. Arora, and R. Ikink, "Cell detachment method using shock-wave-induced cavitation," Ultrasound Med. Biol. **29**(12), 1769–1776 (2003).
15. C.-D. Ohl, M. Arora, R. Ikink, N. de Jong, M. Versluis, M. Delius, and D. Lohse, "Sonoporation from jetting cavitation bubbles," Biophys. J. **91**(11), 4285–4295 (2006).
16. R. Dijkink, S. Le Gac, E. Nijhuis, A. van den Berg, I. Vermes, A. Poot, and C.-D. Ohl, "Controlled cavitation-cell interaction: trans-membrane transport and viability studies," Phys. Med. Biol. **53**(2), 375–390 (2008).
17. H. W. Baac, J. G. Ok, A. Maxwell, K.-T. Lee, Y.-C. Chen, A. J. Hart, Z. Xu, E. Yoon, and L. J. Guo, "Carbon-nanotube optoacoustic lens for focused ultrasound generation and high-precision targeted therapy," Sci Rep **2**, 989 (2012).
18. H. W. Baac, J. Frampton, J. G. Ok, S. Takayama, and L. J. Guo, "Localized micro-scale disruption of cells using laser-generated focused ultrasound," J. Biophoton. doi: 10.1002/jbio.201200247 (2013).
19. H. Won Baac, J. G. Ok, H. J. Park, T. Ling, S.-L. Chen, A. J. Hart, and L. J. Guo, "Carbon nanotube composite optoacoustic transmitters for strong and high frequency ultrasound generation," Appl. Phys. Lett. **97**(23), 234104 (2010).
20. T. Lee, D. Jang, D. Ahn, and D. Kim, "Effect of liquid environment on laser-induced backside wet etching of fused silica," J. Appl. Phys. **107**(3), 033112 (2010).
21. K. R. Rau, P. A. Quinto-Su, A. N. Hellman, and V. Venugopalan, "Pulsed laser microbeam-induced cell lysis: time-resolved imaging and analysis of hydrodynamic effects," Biophys. J. **91**(1), 317–329 (2006).
22. D. G. Shchukin, E. Skorb, V. Belova, and H. Möhwald, "Ultrasonic cavitation at solid surfaces," Adv. Mater. **23**(17), 1922–1934 (2011).
23. T. D. Mast, "Empirical relationships between acoustic parameters in human soft tissues," ARLO **1**(2), 37 (2000).
24. E. Zwaan, S. Le Gac, K. Tsuji, and C.-D. Ohl, "Controlled cavitation in microfluidic systems," Phys. Rev. Lett. **98**(25), 254501 (2007).
25. E. Herbert, S. Balibar, and F. Caupin, "Cavitation pressure in water," Phys. Rev. E Stat. Nonlin. Soft Matter Phys. **74**(4), 041603 (2006).

1. Introduction

Focused ultrasound with high intensity or high peak pressure can produce localized disruptions in terms of acoustic cavitation, streaming, and heat deposition [1,2]. These effects have been broadly utilized for non-contact therapeutic applications such as shockwave lithotripsy [3,4], hyperthermia-based tumor treatment [5–7], and thrombolysis [8,9]. In the local disruption process, cavitational disturbances are of especial interests because they can disintegrate tissues non-thermally (known as histotripsy) [9–12] and facilitate thermal ablation processes collaboratively [12]. Furthermore, the cavitational impacts, together with shock-induced effects, have offered great potentials for *in vitro* cellular engineering in terms of selective cell detachment, patterning, and harvesting for cell-based assays and secondary analyses [13–16]. However, most of these ultrasonic disruptions were available over a bulky focal dimension (typically several mm) due to low operation frequencies (a few MHz) of existing high-pressure transducers [6]. Such dimension is unsuitable not only for performing micro-scale therapies and cellular engineering, but also for exploring microscopic interaction mechanisms with cells in a new regime.

Higher precision has been recently achieved by laser-generated focused ultrasound (LGFU) that simultaneously allows single-pulsed cavitation in a controllable and on-demand manner [17]. High peak pressures of tens of MPa could be tightly focused onto a spot diameter of <100 μm due to inherent high-frequency characteristics of the optoacoustic generation (centered at ~15 MHz with a 6-dB cutoff around 30 MHz). Thus, LGFU-induced disruptions could be demonstrated in a micro-scale regime, enabling single-cell detachment and trans-membrane delivery over a few cells [17,18]. Particularly, acoustic cavitation under LGFU could be delicately controlled with pressure amplitudes near a cavitation threshold. This allowed a tightly confined impact only at the focal center (<60 μm in diameter for a given 6-dB focal spot of 100 μm), barely affecting the peripheral region [18]. Such focal disruption mechanism was partly clarified as originated from micro-jet formation upon bubble collapse. However, detailed processes are unclear yet during bubble growth and collapse.

As compared with conventional low-frequency focused ultrasound, LGFU provides unique opportunities for micro-fractionation of cells, towards high-precision surgery applications, as well as cell patterning and harvesting in an unparalleled manner. It is essential

#187689 - $15.00 USD Received 25 Mar 2013; revised 3 Jul 2013; accepted 10 Jul 2013; published 26 Jul 2013

to investigate such feasibilities and elucidate microscopic disruption mechanisms. Here, we demonstrate that a dense cluster of cultured cells can be fractionated and cleaved with sharpness defined by LGFU. In the micro-cutting process, we give a particular attention on radial disturbances over the peripheral region of focal spot that facilitate cell cluster separation. Then, we investigate LGFU-induced cavitation and shockwaves without cells to clarify surface-mediated mechanisms due to cavitation and shockwaves. Using a laser-flash shadowgraphy, we examine entire processes under LGFU, first to our knowledge, from the focusing of the incident ultrasound to the generation and collapse of bubbles to. These visualize micro-scale disturbances over the focal and the peripheral zones that can be responsible for the cell cluster fractionation.

2. Methods

2.1 Optoacoustic lenses

We used two optoacoustic lenses: one with 12-mm diameter and 11.46-mm radius of curvature for cell experiments, and the other with 6 mm and 5.5 mm respectively for the laser shadowgraphy. Each lens has a carbon nanotube-polymer (CNT) composite film [17,19] on a concave surface, working as an optoacoustic conversion layer. Multi-walled CNTs were grown on fused silica concave substrates by chemical vapor deposition, and then coated by a 20-nm thick Au layer by using an electron-beam evaporation process. The Au deposition further enhances the optical extinction of the as-grown CNT film up to >85%. Finally, the CNT film was spin-coated by polydimethylsiloxane (PDMS). The nano-composite film thickness was ~16 μm (± 20%) on the spherical curvature. The Grüneisen parameter was calculated as 0.72, obtained from the physical properties of PDMS. LGFU has a bipolar waveform with a sharp positive shockfront followed by a broad tensile phase (single pulse duration < 100 ns). It has a center frequency around 15 MHz and 6-dB roll-off points at 7 and 30 MHz, measured by using a broadband fiber-optic hydrophone. The 12-mm lens with a longer focal distance allowed more spacing and convenient ultrasonic alignment with an optical microscope. The optoacoustic lenses were excited with a 6-ns pulsed laser beam (532-nm wavelength; Surelite I-20, Continuum, Santa Clara, CA, USA) with an energy of 20~60 mJ/pulse that allows LGFU to produce cavitation. The laser energy was measured at the lens location. LGFU from the 12-mm lens had 6-dB focal widths of 100 μm (lateral) and 650 μm (axial). The 6-mm lens allowed slightly tighter dimensions of 75 μm and 400 μm, respectively.

2.2 Cell fractionation experiment

An LGFU setup was prepared on an inverted microscope (Fig. 1(a)) [17,18]. The pulsed laser beam (initially, 5-mm diameter) was expanded by 5-fold and collimated. The optoacoustic lens, mounted on a 3-dimensional motion stage, was irradiated uniformly with the enlarged beam. We used a spacer (made of UV-curable epoxy) that is attached on the side of the optoacoustic lens. The bottom surface of the fixed-length spacer easily guides the acoustic focal plane. Once the bottom was made contact with the surface of 4-inch petri-dish, then we slightly lifted up the optoacoustic lens to compensate an offset due to the culture substrate thickness. This located the ultrasonic focus exactly on the cells. The halogen lamp was used as an illumination source for optical imaging. We used a notch filter (centered at 532-nm wavelength; Edmund Optics, Barrington, NJ) to block the scattered laser from being incident to the detector. The images were recorded by a charge-coupled device (CCD).

SKOV3 ovarian cancer cells were cultured on polymer-coated glass substrates with two different confluences [17]. First, a densely packed cell cluster was prepared for the ultrasonic cutting experiment. A surface-modified polymer film was used for adhesion promotion of the high-density cells. The other cells were cultured in a relatively low density to form a sparse network on the substrate. All the process of ultrasonic alignment and cell detachment were confirmed microscopically.

#187689 - $15.00 USD Received 25 Mar 2013; revised 3 Jul 2013; accepted 10 Jul 2013; published 26 Jul 2013

2.3 Shadowgraphic imaging

A laser-flash shadowgraphy setup was prepared without the optical microscope (Fig. 1(b)). The same pulsed laser was used as a pump for the optoacoustic excitation. A probe beam (UV-pumped dye laser, 1-ns pulse duration) was chosen to provide fast temporal resolution and sufficient illumination for high-contrast imaging along the laser path [20]. A fiber-optic hydrophone (125-μm diameter) was placed at the focal zone as a guidance of ultrasonic focus as well as a supporting boundary to induce cavitation. We used a glass supporter to firmly hold the thin fiber (glued with a UV-curable epoxy). The optoacoustic lens (6-mm diameter) and the glass supporter were mounted to 3-dimensional motion stages, respectively. LGFU was measured using the fiber-optic hydrophone with a broad bandwidth up to 75 MHz.

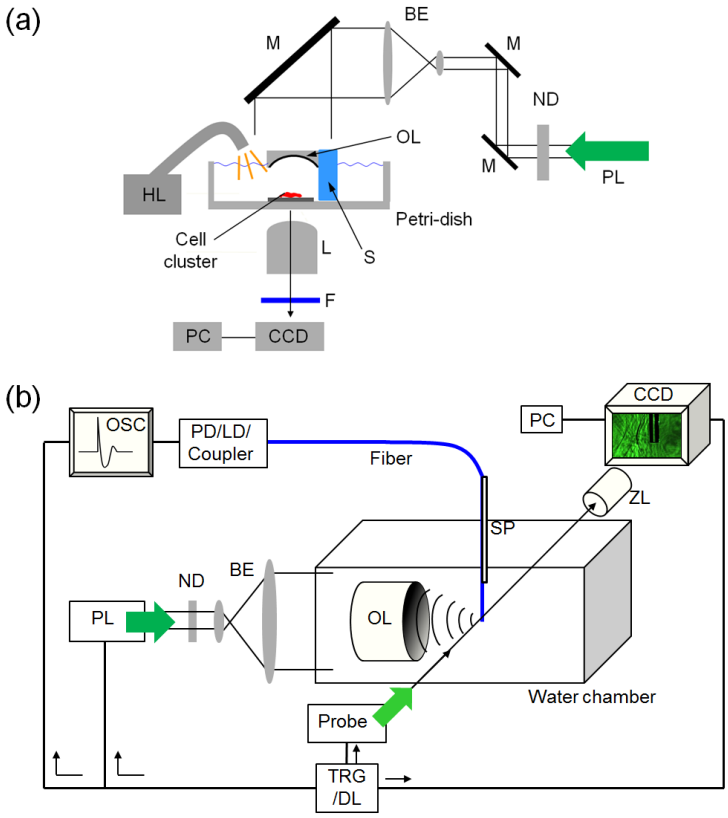

Fig. 1. Experimental schematics. (a) A setup for micro-fractionation of cell clusters by LGFU. The setup was prepared on the inverted microscope (BE: beam expander, F: optical filter, HL: halogen lamp, L: objective lens, M: mirror, ND: neutral density filter, OL: optoacoustic lens, PL: Nd:YAG pulsed laser beam (6-ns pulse width), S: supporting frame,). (b) A shadowgraphic imaging setup (LD: laser diode, OSC: digital oscilloscope, PD: photodetector, Probe: probe laser beam (1-ns pulse width), SP: supporting plate, TRG/DL: trigger and delay-generator unit, ZL: zoom lens).

Although the fiber detects the pressure in a perpendicular alignment to the optoacoustic lens axis as shown in Fig. 1(b), the hydrophone sensitivity was sufficient to find the ultrasound focus. Once the focal spot was located, then the fiber was slightly moved down to work as a cavitation boundary. Simultaneously, the cylindrical fiber was used as a thin optical object in the perpendicular direction to find a shadowgraphic focus. A pulse repetition rate of the probe beam was <20 Hz. Using the trigger-and-delay unit (TRG/DL) (DG535, Stanford Research Systems, Sunnyvale, CA, USA), we synchronized the pump beam, the probe beam, the oscilloscope, and the CCD. A proper time delay was given between the pump and the probe

#187689 - $15.00 USD Received 25 Mar 2013; revised 3 Jul 2013; accepted 10 Jul 2013; published 26 Jul 2013

pulses to obtain an instantaneous image in each step of LGFU-induced disruption processes. Finally, the shadowgraphic images were recorded by the CCD.

3. Results and discussion

Using LGFU, we cut a chunk of cell cluster cultured on a glass substrate. The laser energy (E) of >50 mJ/pulse was used to generate the focused ultrasound, resulting in pressure amplitudes of >50 MPa in the peak positive and higher than the cavitation threshold in the peak negative (estimated amplitude: >20 MPa). The laser energy is >4.5 fold higher than the threshold value (E_{th} = 11 mJ/pulse for the 12-mm optoacoustic lens) to generate the cavitation. In this regime, a generation rate of cavitation per a single LGFU pulse was ~100% on the glass substrate.

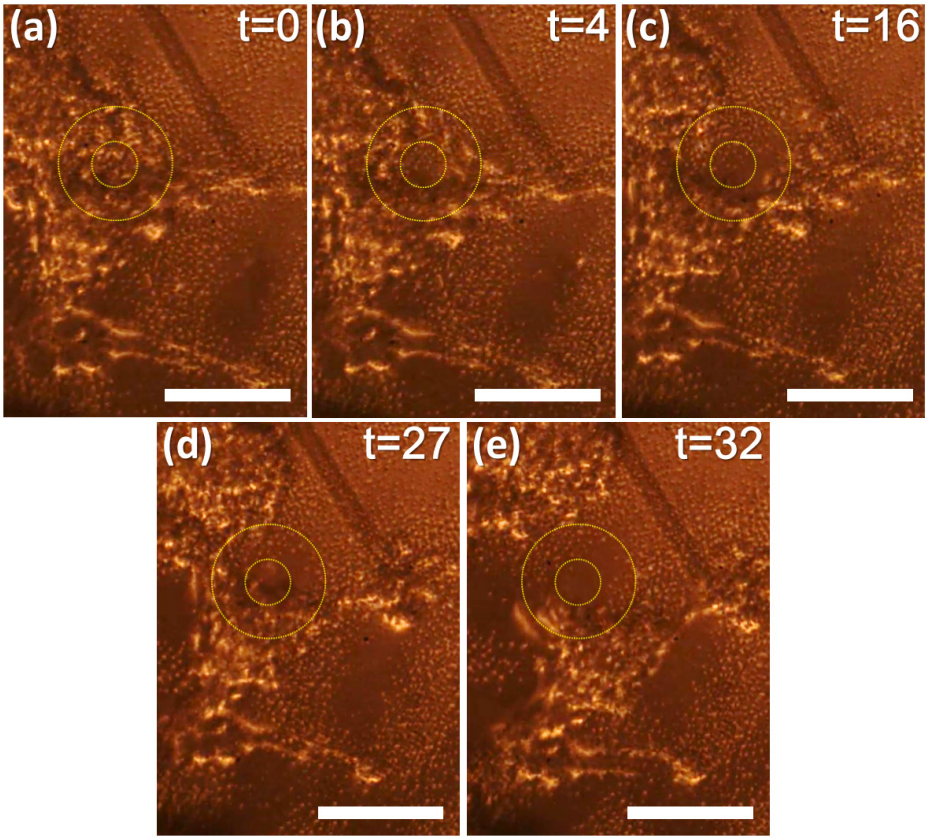

Fig. 2. Demonstration of micro-fractionation by LGFU (Media 1) (scale bar = 100 μm). The LGFU spot is fixed while the cell culture plate is slowly moved to the upper-right direction (a-e). For convenience, the disruption zones are guided by the inner and outer circles (35 and 90 μm in diameter, respectively). A captured time (t) is shown on the right-top corner (unit: second): (a) The cultured cell cluster is shown with a target spot; (b) Under LGFU, the cluster is fractionated primarily at the focal center; (c) The prolonged exposure of LGFU enlarges the fractionated zone over the periphery; (c-e) As we move the cluster, LGFU finally cleaves it into two pieces.

Figure 2 shows a sequential process of ultrasonic cleaving, displayed as a series of photographs captured from video recording (Supporting information; Media 1). The LGFU spot is guided by the concentric circles that indicate a focal center and a periphery. These were separated in our convenience according to cell fractionation behaviors. Under the LGFU exposure in Fig. 2(b), the cell cluster was disintegrated mostly within the inner zone. Then, the prolonged LGFU exposure over Fig. 2(c) and 2(d) swept away the peripheral cells, noticeably widening the damage zone. Here, we could observe two phenomena. First, individual cell detachment was frequently observed at the focal center. The cells at the focal

#187689 - $15.00 USD Received 25 Mar 2013; revised 3 Jul 2013; accepted 10 Jul 2013; published 26 Jul 2013

center are exposed to the sharply focused shockwave (>50 MPa) and cavitational disturbances in terms of a collapse-induced liquid jet [15] and secondary shockwaves toward the focal center. Second, we could also observe that the cells in the peripheral region (*i.e.* outer circle) are pushed away radially from the focal center, rather than individually detached. This outward effect can be attributed primarily to a cavitation-induced liquid jet along the wall [15,16]. Such "pushing effect" in the periphery facilitated the cleaving process. We note that the peripheral effect was distinctively observed after the focal fractionation shown in Fig. 2(b). This means that the peripheral disruption requires continual and repetitive LGFU exposure than at the focal center (a pulse repetition rate of LGFU = 20 Hz). During the steps of Fig. 2(c)–2(e), the cell culture plate was moved slightly to the upper-right direction. The cluster was completely cut after 32-second exposure as shown in Fig. 2(e). From the results of Fig. 2, we could confirm that the cell cluster can be ultrasonically fractionated and divided by collateral disruptions over the center and the periphery of LGFU spot.

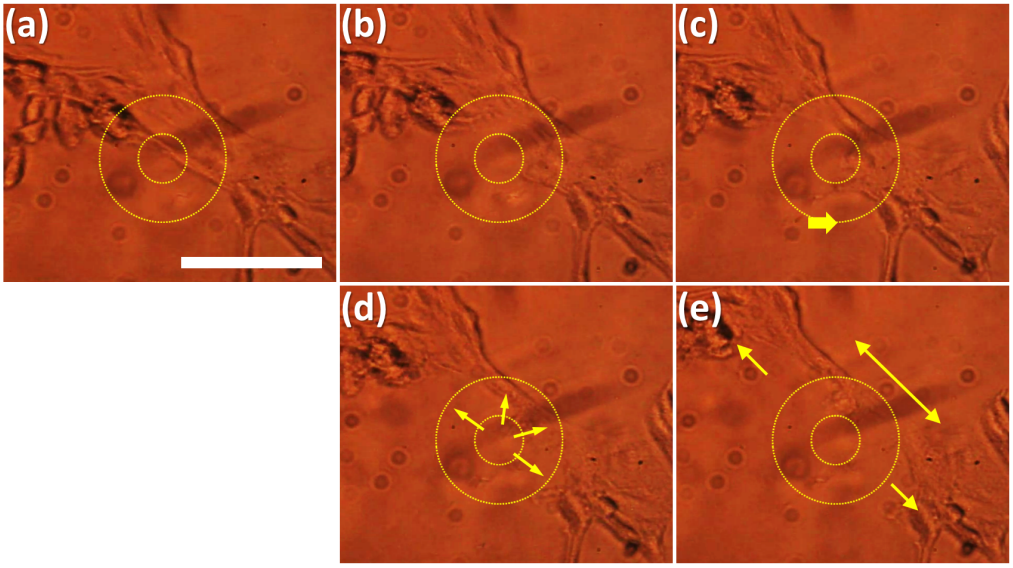

Fig. 3. Micro-fractionation process in a sparse cell network that is used for distinctive morphology deformation (scale bar = 100 μm; inner and outer circle diameters = 35 and 90 μm; time *t* (second)): (a) The LGFU spot was positioned at the cell-cell junction; (b) In a short time, the junction is sharply cut by LGFU at the focal center; (c) The spot is re-positioned slightly to the rightward direction; (c)-(e) The spot stays at the same position to observe the peripheral disruption effects under prolonged LGFU. The cells are pushed away along the radial directions (arrows in (d)), and their retreatment is clearly shown in (e) (compare with (c)), indicated by two small arrows. Also, the cell-cell connection is pulled away along the bi-directional arrow.

It is interesting to note that the cells exhibit different behaviors with respect to their location under the ultrasound focal zone. We further confirmed the outward pushing effect on the peripheral region, using cells cultured sparsely on the substrate (Fig. 3(a)). These spread cells, cultured with low density (<200 cells/mm^2), allow us to easily observe fine variation on their morphology that can be overlooked in the densely packed cells. LGFU was produced using E = 20~25 mJ/pulse. As shown in Fig. 3(b), the cell-cell junction was quickly disconnected within the central zone. In Fig. 3(c), the LGFU spot was re-positioned by moving the cell culture plate. The spot stayed at almost the same position during the steps of Fig. 3(c)–3(e). In these steps, the cell morphology was deformed along the radial directions (arrows in Fig. 3(d)). The comparison of Fig. 3(c) and 3(e) clearly reveals that the cells were deformed retreating outwards as indicated by two small arrows in Fig. 3(e). The cellular junction is stretched by these radial forces (a bidirectional arrow in Fig. 3(e)). The cell deformation was observed even over 300-μm diameter in Fig. 3(e). Such damage dimension

#187689 - $15.00 USD Received 25 Mar 2013; revised 3 Jul 2013; accepted 10 Jul 2013; published 26 Jul 2013

varied along individual cell morphology and adhesion on the substrate. Again, the relatively slow process over 10~20 seconds means that the cells are swept away by the repeated disturbances under the prolonged LGFU exposure.

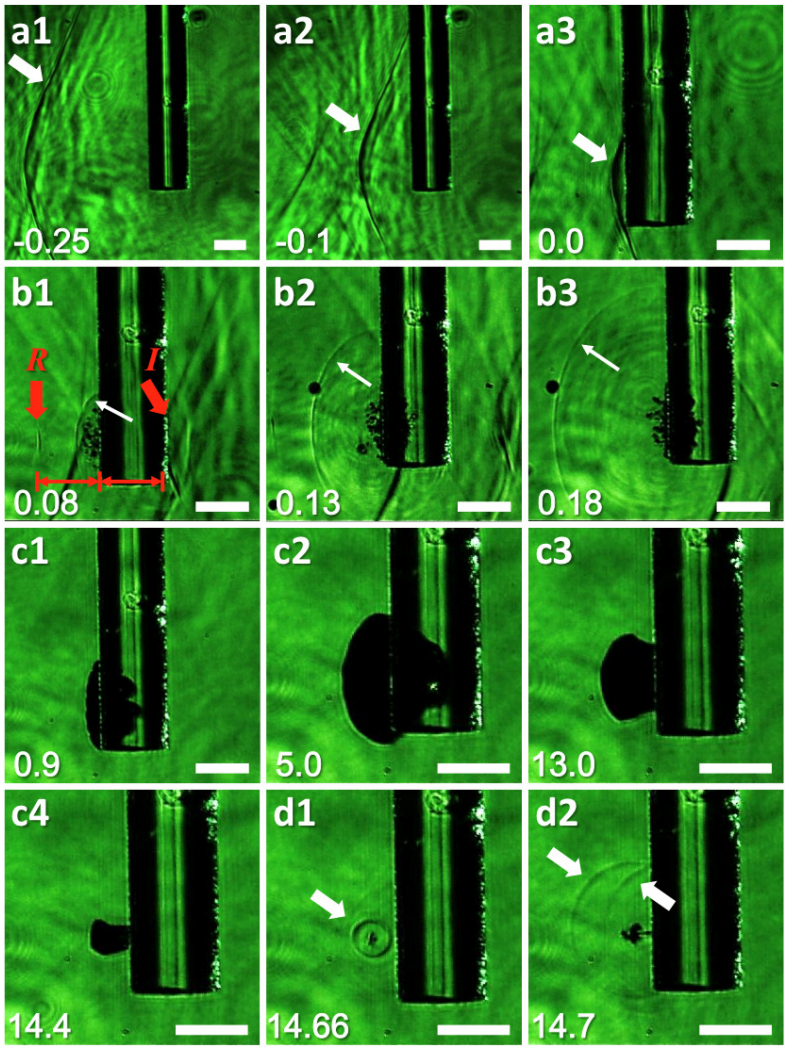

Fig. 4. Shadowgraphic imaging of LGFU-induced disruptions (all scale bars: 100 μm). Instantaneous images are shown sequentially. A captured time is shown on the left bottom (unit: μs) as relatively defined from the moment of cavitation inception. The fiber thickness is 125 μm for all figures: (a1-a3) Incidence of LGFU from the left to the right. The wavefronts are indicated by the arrows; (b1-b3) Tiny bubbles generated under LGFU with the outgoing pressure wave (thin red arrow); (c1-c2) A cloud formation by the merged bubbles; (c3-c4) Shrinkage steps; (d1) A collapse-induced shock is shown as the spherical wavefront (arrow); (d2) Shock propagation is shown by the left arrow (a direct outgoing wave) and the right arrow (a reflected wave from the substrate).

Although the cell clusters were controllably and sharply cleaved by LGFU, the fractionation mechanisms need further explanation. Moreover, even without cells, LGFU-induced disruption processes have not been completely understood yet. Here, we performed a control experiment without cells to elucidate the background mechanisms mainly associated with cavitational disturbances. We used a laser-flash shadowgraphic technique to fully visualize instantaneous microscopic processes under LGFU and to provide reasonable hypotheses for the focal and peripheral disruptions.

#187689 - $15.00 USD Received 25 Mar 2013; revised 3 Jul 2013; accepted 10 Jul 2013; published 26 Jul 2013

Entire procedures of the LGFU-induced disruption are shown in Fig. 4, from the incidence of the focused ultrasound wave successively to the bubble collapse moment. LGFU was incident from left to right onto the glass fiber (horizontal thickness = 125 μm). The LGFU axis is perpendicular to the shadowgraphic images. The top row (a1-a3) shows the LGFU propagation process before the inception of cavitation. As the shock front of LGFU has >50 MPa in the peak amplitude, local variation of water density was clearly visualized with high contrast. The second row (b1-b3) shows an initial stage of cavitation containing tiny bubbles. Formation of these bubbles can push out the surrounding water, producing an outgoing pressure wave. Note that the generated wavefront (b1) agrees with the region of tiny bubbles. Particularly, we marked two wavefronts at this moment. The incident wavefront propagating rightward (marked as *I*) appears as a dark line that is almost interfaced with the right fiber surface. The reflected wavefront (marked as *R*) is located in the left, which has the same propagation distance with that of the incident wave from the nucleation boundary (*i.e.* the left fiber surface). As shown here, there is a time delay between the bubble-induced outgoing pressure wave (thin white arrow) and the incident wave (*I*). This can be calculated as ~40 ns through the image that approximately agrees with the temporal difference between positive and negative phases of the bipolar LGFU waveform. This means that the bubble-induced outgoing wavefront is due to the negative pressure exerting on the boundary, rather than the direct scattering of the incident shockwave. While the initial evolution of cavitation takes places over a short period of a few 100 ns, the following steps are progressed over a relatively long duration (c1-c4) along with the bubble lifetime, 14~15 μs in this example. After the growth and shrinkage steps, we observed the collapse-induced shock emission (d1) that propagates to the outgoing direction. As the right half-portion of this spherical shockwave is reflected from the substrate, two shock fronts appear in d2.

With the visual evidences of focal and peripheral disruptions provided by the high-speed shadowgraphy, we can reasonably explain the cell fractionation mechanisms. Apparently, the cells at the focal center are exposed to stronger disturbances than those at the surrounding zone. In addition, micro-jetting can be formed as the merged bubble cloud is collapsed. This produces local stresses towards the focal center [15,18]. Since all these effects are concentrated at the focal center, the single cells could be individually and sharply detached from the cluster.

The outward pushing mechanism over the peripheral region can be explained by a liquid jet along the wall. Following the bubble collapse, a transient liquid jet can be formed and directed toward the substrate surface, then spreading radially along the wall. Ohl *et al.* [15] have reported that cultured cells can be detached by this wall jet-induced shear stress due to bubble collapse. It is known that impacts of such transient fluid depend on the location of the bubble above the surface. Dijkink *et al.* [16] could determine the radius of cell detachment zone by bubble collapse (R_{det}) as a function of a stand-off distance of the bubble ($\gamma = h/ R_{max}$ where h is the distance of the bubble center to the wall and R_{max} is the maximum radius of the bubble). Similarly, from Fig. 4(d1), we can obtain γ ~0.39 for LGFU-induced bubble, which results in $R_{det} = 0.72R_{max} = 65$ μm [16]. This means that cells within the diameter of $2R_{det}$ would undergo significant wall shear stress due to the liquid jet. Figure 2 shows that the ultrasonic cleaving process substantially occurs within the diameter of $2R_{det} = 130$ μm that is placed under the wall jet impact. The wall jet would lead to complete cell detachment within $2R_{det}$ if cells were monolayer-cultured [15,16]. However, the cells in the cluster can be mechanically more resistive due to interconnections with neighboring cells and substratum, significantly increasing a critical shear stress for cell detachment [21]. In Fig. 2, indeed, the outward pushing effect on the peripheral zone was primarily observed with less detachment. Thus, the wall shear stress can be responsible to the outward pushing effect over the periphery of focal spot.

It should be also noted that the wall shear stress gradually decreases over the radial distance. Therefore, cells in the vicinity of the detachment zone ($R > R_{det}$) can still be influenced by the shear stress. In Fig. 3, we used the sparsely cultured cells (mono or a few layers; cell density <200 cells/mm^2) that can respond to delicate disturbance. We could

#187689 - $15.00 USD Received 25 Mar 2013; revised 3 Jul 2013; accepted 10 Jul 2013; published 26 Jul 2013

observe cell deformation over the region of $R > R_{det}$ (= 65 μm) (Fig. 3). Such delicate change over the broad zone was not easily observed in the cell cluster.

We have confirmed that LGFU-induced cavitation can produce various disruption mechanisms during bubble formation and collapse. Together with shock-induced effects by the incident LGFU, the cavitational disruptions are readily available for micro-patterning and harvesting of cultured cells. In these applications, a rigid substrate plays both roles as a nucleation boundary for micro-bubbles and a cell culture plate. However, without such rigid entities, the threshold pressure for cavitation would increase significantly in the high-frequency regime of LGFU [22]. Especially in tissue environments considered as soft boundaries, the LGFU-induced cavitation needs further investigation. An intrinsic cavitation threshold (P_{int}) to induce micro-bubbles depends on acoustic properties of objects (*e.g.* tissues [9,23]) and their morphological characteristics [22,24]. In some case, the cavitation requirement can be relaxed, for example, in fat (P_{int} ~−16 MPa at 1-MHz frequency) as compared in water (−27 MPa) and kidney (−30 MPa) [9]. The threshold can be more complicated as external variables are taken into account, such as temperature and initial densities of nucleation sites in the surrounding liquid [25].

4. Conclusions

We demonstrated ultrasonic micro-fractionation of cell clusters *in vitro* environment. Using LGFU, we could cleave a densely packed cell cluster with ultrasonic sharpness of 100 μm. The fractionation process was differentiated by the focal and the peripheral regions of LGFU spot. The cells were sharply disintegrated from the cluster at the focal center. In addition to the focal fractionation, the overall ultrasonic cutting process was facilitated by the peripheral effect that pushes away the surrounding cells out of the focal zone. The peripheral disturbances were further confirmed using a sparse cell network. The laser-flash shadowgraphic imaging successfully visualized LGFU-induced shockwaves and cavitation, providing detailed processes of bubble inception, growth, collapse, associated jetting and shock emissions. These could be used as supporting evidences to reasonably explain cell cluster fractionation mechanisms. Particularly, the outward pushing effect was explained by the wall shear stress that makes primary impacts within the diameter of $2R_{det}$ = 130 μm and gradually spreads into the vicinity. We expect that LGFU can be used as a non-contact, non-thermal modality for cellular and tissue applications such as ultrasonic cleaving, patterning, harvesting, trans-membrane molecular delivery, and potentially high-precision surgery in future.

Acknowledgments

This work is supported by the National Science Foundation. The authors would like to thank Jong G. Ok and Prof. A. John Hart (University of Michigan) for their help for CNT lens fabrication, and Yu-Chih Chen and Prof. Euisik Yoon (University of Michigan) for providing cultured cells. The authors also wish to acknowledge Prof. Zhen Xu (University of Michigan) for generously allowing us to use a fiber-optic hydrophone for measuring the focused ultrasound.

#187689 - $15.00 USD Received 25 Mar 2013; revised 3 Jul 2013; accepted 10 Jul 2013; published 26 Jul 2013